Surface integrity of SLM manufactured meso-size gears in laser shock peening without coating

Pathak, S., Böhm, M., Kaufman, J., Kopeček, J., Zulić, S., Stránský, O., Shukla, A., Brajer, J., Beránek, L., Radhakrisnan, J., Rostohar, D. & Mocek, T

Surface integrity of SLM manufactured meso-size gears in laser shock peening without coating

Sunil Pathak [a,*], Marek Böhm [a,b], Jan Kaufman [a], Jaromír Kopeček [c], Sanin Zulić [a], Ondřej Stránský [a,d], Ashish Shukla [e], Jan Brajer [a], Libor Beránek [d], J. Radhakrisnan [f], Danijela Rostohar [g], Tomáš Mocek [a]

[a] *HiLASE Centre, Institute of Physics of the Czech Academy of Sciences, Czech Republic*
[b] *Czech Technical University in Prague, Faculty of Nuclear Sciences and Physical Engineering, Czech Republic*
[c] *Institute of Physics, Czech Academy of Sciences, Prague, Czech Republic*
[d] *Czech Technical University in Prague, Faculty of Mechanical Engineering, Czech Republic*
[e] *Atlas Skilltech University, Navi Mumbai, Maharashtra, India*
[f] *E.T.S. Ingenieros Industriales, Polytechnical University of Madrid, C/José Gutiérrez Abascal, 2, 28006 Madrid, Spain*
[g] *Institute for Advanced Manufacturing and Engineering, Coventry University, CV6 5LZ, UK*

ARTICLE INFO

ABSTRACT

The present work aimed to improve the surface integrity of the selective laser melting manufacturing (SLM) manufactured 10 mm sized meso gears using the unconventional Laser Peening without Coating (LPwC) technique. To accomplish LPwC on meso gears low energy in the range of 200 mJ to 1000 mJ at 10 Hz were applied underwater in the gear root and fillet gap generating significant surface compressive residual stresses (from +73 MPa to −298 MPa). Besides the surface, residual stresses, average surface roughness (Ra), arithmetical mean height (Sa) and parameters of the material ratio curve were also considered as a part of the study. Notable improvement was achieved in Sa, as it improved over 50 % while considerable improvement in Ra and the material ratio curve parameters has also been observed. Scanning electron microscopy confirmed that the void and porosity seen in the unpeened gears were filled. The electron backscatter diffraction analysis confirms the grain refinement in LPwC region up to 100 μm depth. It was observed that multifold dislocation occurs within the grain, and dislocation generates sub-grain. The sub-grain formation substantially inhibits further nucleation and crack propagation owing to an increase in grain boundary density. Such improvement justifies the set objectives, and the outcome of this research will pave a foundation to improve the overall performance of the micro/meso parts using the LPwC process.

1. Introduction

Micro and miniature components are vital players in manufacturing industries, especially aerospace, automobile, electronics, telecommunications, information technology, and medical industries. The high demand for smaller and functional appliances, machines, and parts in worldwide economies is increasing rapidly owing to their modest volume, lightweight, portability, and reliable efficiency. Components with a size spectrum from 1 to 1000 μm are referred to as micro-components [1]. They are frequently used in several micro-devices, micro-systems, and micro-products. In the recent decade, attention has been paid to producing these products [1]. The development of additive manufacturing (AM) has helped industries and mankind significantly, especially when designing and manufacturing an intricately shaped geometry [2,3]. AM allows flexibility to the industries to print the part for specific needs and applications. However, the poor surface properties in terms of surface quality (SQ) and surface integrity (SI) of the AM components are still a crucial challenge for industries [3]. The surface quality fundamentally displays the manufactured part's exterior surface, such as; surface texture, roughness, lays, laps, tears, pits, and other geometrical deviations. Whereas surface integrity reflects the interior of the surface typically 0.1–0.5 mm below the surface of the manufactured part, this includes microstructural alterations, intergranular changes, heat affected zone, microcracks, hardness alteration, residual stresses,
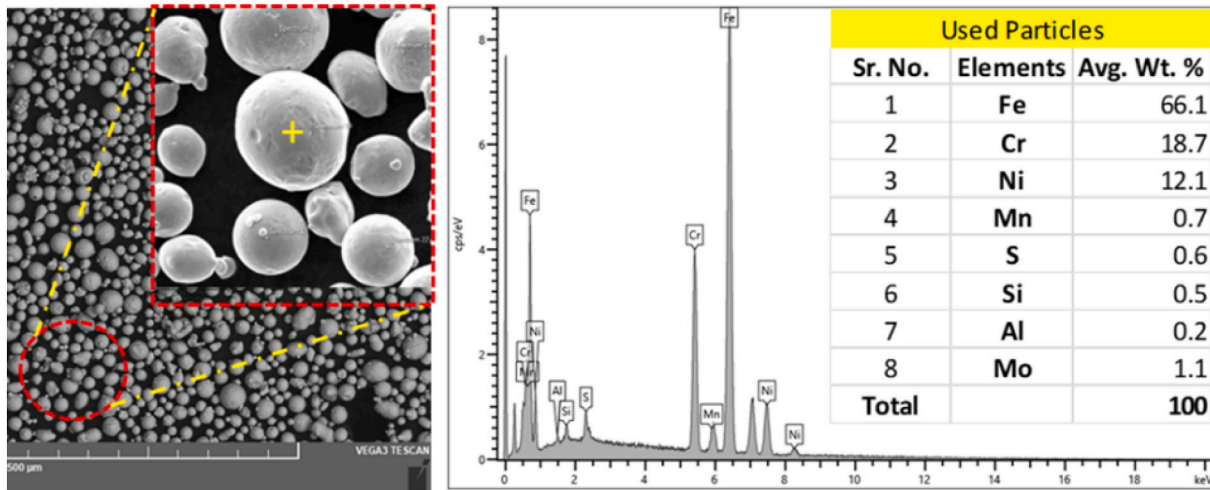
Fig. 1. Scanning electron microscopy of the powder and chemical composition of powder used for SLM.

material inhomogeneity, etc. [1,4]. Typically for an engineering application where fatigue failures play a vital role, the demand for precision manufacturing (i.e. excellent SQ and SI) is high, as most of the failures occur due to poor SQ and SI of the component. Out of the various parameters of SQ and SI; roughness, residual stress (compressive), microstructure, and microhardness plays a vivacious role in deciding the service life of any AM or conventionally manufactured components. The control over SI add extra cost to the manufacturing, therefore it must be considered to manufacture highly stressed part used in applications where human safety, high cost, and predictable component life are of major concern [5]. Surface integrity helps describe and control the various possibilities of alterations that may occur within the surface layer of any engineering part during manufacturing. This also influences the materials' properties and the manufactured part's service life performance [4,6]. To improve the SQ and SI, several post-processing operation such as machining, finishing, polishing, sand blasting, shot peening, laser shock peening etc., are commonly used by industries. Recently, laser shock peening has gained attention from the industries and researchers to improve the SQ and SI of the AM parts. LSP employs high-energy (>1 J) nanosecond laser pulses to generate large, localized pressure on metal surfaces. Shock waves propagate into the metal, causing plastic deformation and generation of compressive residual stresses, which positively impact the material's mechanical properties, particularly fatigue life. At its core, LSP is a cold working process which means that no heat is typically transferred to the material, only mechanical pressure [4–6,7]. During the process, a laser pulse hits the surface, creating plasma. The plasma expansion is then confined to the surface by a thin water layer, significantly increasing the pressure created. LSP is usually performed with a protective tape over the workpiece surface or performed underwater without taping for a certain application to absorb the laser pulse heat and protect the underlying material from heat effects [7]. Afterwards, plasma pressure is converted into shock waves and plastic deformation occurs once the shock wave stress overcomes the metal yield strength. This plastic deformation causes crashing/crunching of the grains and microstructure refinement. The depth of plastic deformation and the imparted compressive residual stresses and refined microstructure depends on the material, laser induced shock pressure, and laser spot size. Based on the chosen laser process parameters the affected depth can be engineered for various applications [8]. Mukai et al. [9] first tested the laser peening without coating (LPwC) technology to provide large shock wave pressures with low energy lasers and small spot diameters. Although the LPwC is not examined over stainless steel material and a very few literature has reported the effect of LPwC on stainless steel alloy. Nataraj and Swaroop [10] studied in detail the effect of LPwC on SS304; they discussed the

microstructural improvement in their experiments and identified the transformation of high-angle grain boundaries to low-angle grain boundaries after LPwC along with the improvement in compressive residual stresses. Various other researches have been done on LPwC and LSP on different materials such as Ti-6Al-4V Alloy [11,12], Ti 15V-3Al-3Cr—3Sn alloy [13], Al-Si10-Mg [14] etc. Most of the studies were limited to macro size components, and very few attempts have been made on micro/meso size components, especially those made with SS316L and AM processed. Based on the above discussion, in the present work meso sized (maximum outside diameter 10 mm) [15] spur gears were manufactured using selective laser melting (SLM) and further post-processed to modify the surface quality (surface roughness, materials distribution curves, and surface morphology) and surface integrity (residual stresses and microstructure) by applying underwater laser shock peening without coating (LPwC). The underwater treatment for the meso size gears was done due to the complexity involved in the taping near the fillet gap and root of the meso-size gear. The area of peening was selected based on the literature on gear engineering that suggests that the failure in gears initiates from the root and thus, it is essential to safeguard the root to improve the overall life of gears. Performing LPwC treatment at different laser pulse energies provided inside to the physical behaviour of the process.

2. Materials and methods

2.1. SLM of miniature gears

Selective laser melting (SLM) is one of the most advanced additive manufacturing (AM) technologies in use today. In SLM, the metallic powder is fused with a high-intensity laser in a layer-by-layer process to create complexly formed geometry. The intricacy of part designs can be beyond the comprehension of the layman's thinking, and the creation of such designs using conventional manufacturing or machining processes can be extremely challenging or nearly impossible. As a reliable and promising AM technique, SLM has the advantages of minimal material waste volume, improved process control and accuracy, dense material creation, and shorter production cycles. Although SLM has many benefits, there are still many unresolved research questions, such as those involving inhomogeneity in material deposition or during the layer-by-layer fabrication of components, which leads to undesirable microstructures and excessive surface roughness. Columnar structures and larger grain sizes are produced by the unidirectional solidification of fused material caused by a thermal gradient in the build directions [4,16]. The mixture of coarse grain sizes in the built-up directions leads to undesirable anisotropic mechanical properties and constituents as a

Table 1

Gear design and SLM parameters.

Parameters	Spur gear
Number of teeth	10
Normal module	0.8
Transverse module	0.8
Pressure angle (degree)	20
Transverse pressure angle (degree)	20
Helix angle (degree)	0
Outside diameter (mm)	9.6
Pitch circle diameter (mm)	8
Base circle diameter (mm)	7.5
Root diameter (mm)	6
Tooth thickness (mm)	1.25
Bore diameter (mm)	4
Height of hub (mm)	5
Hub outer diameter (mm)	6

SLM parameters	
Slice thickness	0,02 mm
Laser focus diameter	0,055 mm
Laser speed	675 mm/s
Laser power	150 W
Hatch distance	0,1 mm

limitation of the SLM process.

Mezo-sized components which are usually characterized by their dimensions being larger than 1 mm but not exceeding 10 mm can be printed in the same fashion as larger-scale components. However, the mentioned limitations remain the same. Some AM technologies are more suitable laser powder bed fusion (L-pbf) as they are focused on better

detail than others such as direct energy deposition (DED) where the focus is drawn more to higher deposition rates. For this reason, this work focuses on L-pbf. Connected walls of thickness <0,4 mm, individually standing walls of thickness <0,5 mm, unsupported overhangs over 0,5 mm, bridges of >2 mm, and holes of <1,5 mm diameter are usually tricky to print, and it is recommended to avoid these design features if possible (general recommendation for direct metal laser sintering). The L-pbf printer itself is always limited physically by its laser source, the quality of the beam and minimum spot diameter obtainable respectively, regardless of the size of the component which is being printed.

Furthermore, the ISO standard 2768 has defined required tolerances of dimensions that are not specified on the technical drawing based on one of the grades (f, m, c, v). The requirements are relative to the dimension itself describe a small dimension (6–30 mm) has a smaller tolerance (±0.1 mm for grade f), however, the printer operates with the same precision regardless of the size of the manufactured component (with the exception related of dimensional differences coming from the warpage of the part). For the manufacturing of miniature gears with SLM stainless steel 316L in powder form has been used, the powder used in the present work was in used condition, and the scanning electron microscopy of the powder and chemical composition has been presented in Fig. 1. Truprint 1000 model by Trumpf has been used to manufacture miniature gears. The details of gear geometry and SLM parameters have been presented in Table 1. A schematic of SLM has also been presented in Fig. 2.

2.2. Laser shock peening without protective coating (LPwC) and characterization techniques
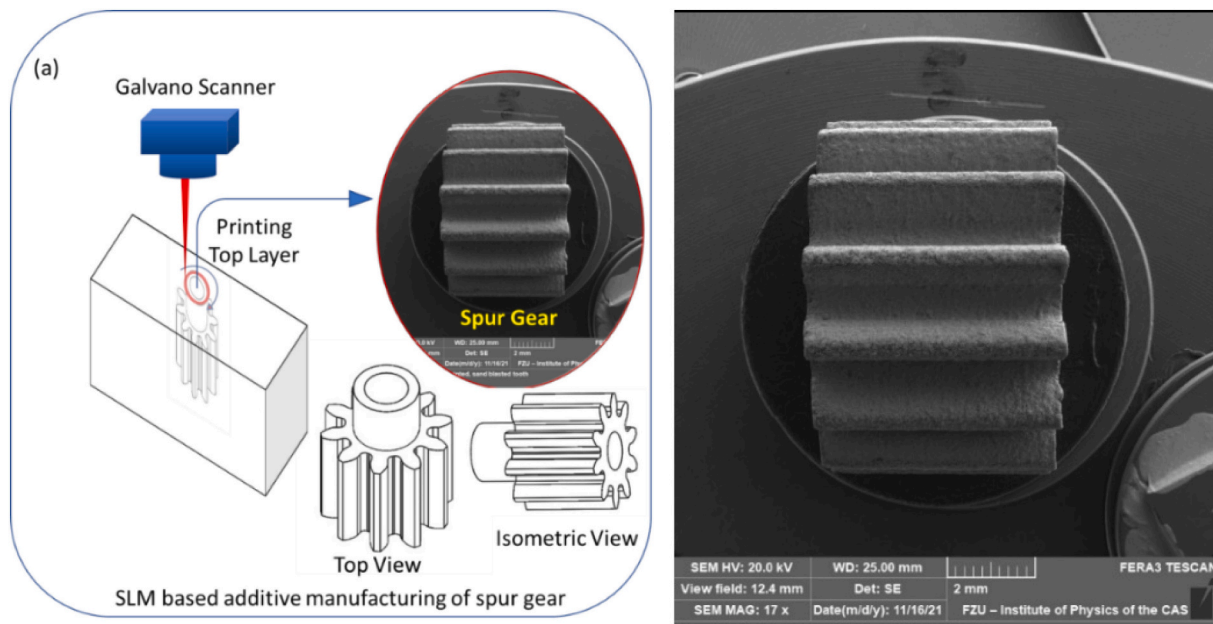
The laser shock peening without protective coating (LPwC)

Fig. 2. Schematics of SLM process.

Table 2

Litron laser with for circular hat top beam profile and wavelength 532 nm used for LPwC.

Energy (mJ)	Pulse duration (ns)	Rep rate (Hz)	Spot size (cm)	Spot area (cm^2)	Laser fluence (J/cm^2)	Overlap (%)	Density (W/cm^2)	Peak density (GW/cm^2)
200	15	10	0.1	7.85×10^{-3}	25.46	90	254.65	1.70
400	15	10	0.1	7.85×10^{-3}	50.93	90	509.3	3.40
600	15	10	0.1	7.85×10^{-3}	76.39	90	763.94	5.10
800	15	10	0.1	7.85×10^{-3}	101.86	90	1.02e+3	6.79
1000	15	10	0.1	7.85×10^{-3}	127.32	90	1.27e+3	8.49
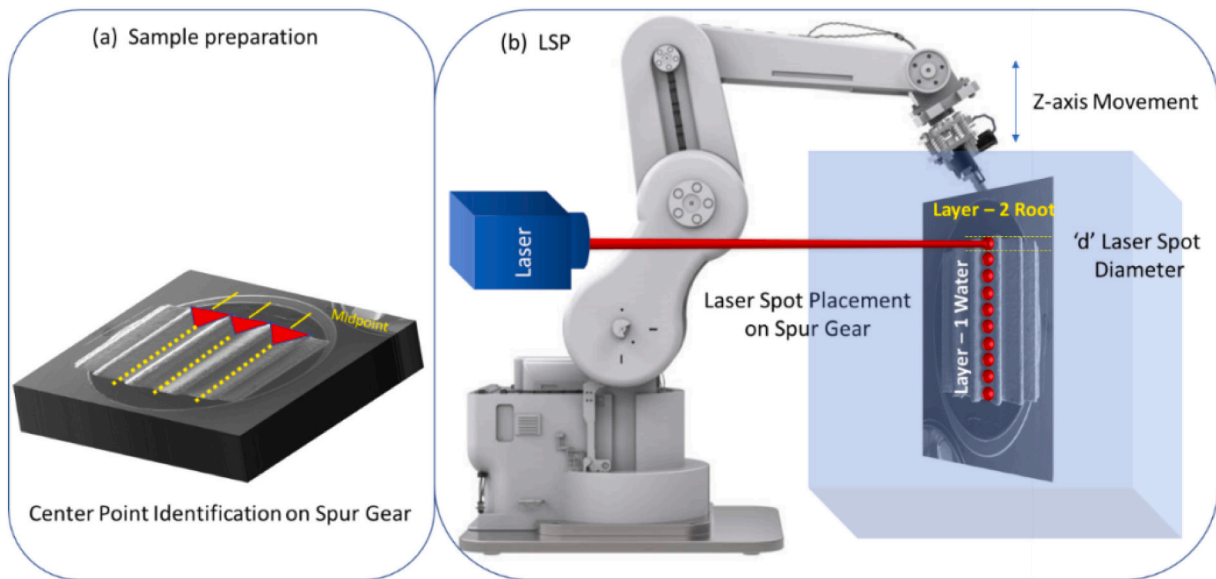
(a)
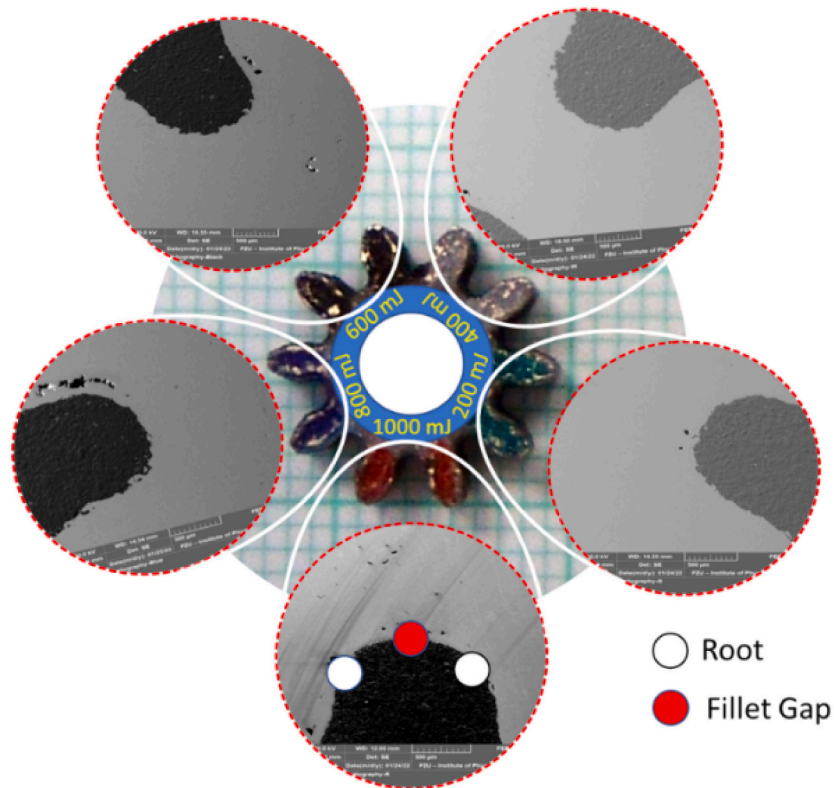
(b)

Fig. 3. Schematic arrangement for (a) LPwC of miniature gears; and (b) Photograph representing the peening zones.

treatments were applied using the flash lamp pumped Nd:YAG laser system Litron operating at 10 Hz repetition rate. In this case, the fundamental wavelength of 1064 nm was converted to 532 nm using a second harmonic generation to allow propagation underwater. The pulses have duration of 15 ns with circular top hat beam profile. In the present work, laser energy was varied at five different levels from 0.2 J to 1 J, while the other parameters such as spot size as 1 mm, overlap as 90 %, and repetition rate as 10 Hz were kept constant. Explanatory details of laser parameters used for present experiments are presented in

Table 2. A schematic depicting the LPwC arrangement has been presented in Fig. 3(a). The targeted zone for the miniature gear was the root and fillet gap to ensure that the flank geometry of the gear will not get altered with the effect of LPwC. Majority of the failures in the gears initiate from the root and propagate further to eventually crack initiation and final rapture [15]. A representation of LPwC zone is presented in Fig. 3(b). Surface residual stress, surface roughness, and surface morphology have been measured on samples before and after LPwC. The surface stress measurements were done with an X-ray diffractometer

Table 3
Details of residual stress measurements before and after LPwC.

Experiment number	Energy (J)	Laser fluence (J/cm²)	Residual stresses in (MPa)	
			Unpeened spur gear in (MPa)	LPwC processed spur gear in (MPa)
1	0.2	25.46	+73 MPa	−191.4
2	0.4	50.93		−108.5
3	0.6	76.39		−298.9
4	0.8	101.86		−202.4
5	1	127.32		−197.8

(XRD) RIGAKU AutoMATE II using the $\sin^2\psi$ method. In this method, several Bragg peak measurements are taken at different tilts psi(ψ) where ψ is the angle between the sample's normal and the diffracting plane's normal. The Bragg peak position is linked with the inter-planar spacing (d), and when anisotropic strain is present, d becomes angle dependent which causes the shift of the Bragg peaks measured at different ψ. The stress is then calculated by fitting the peak position data in the d versus $\sin^2\psi$ plot using X-ray diffraction elastic constants of the material. The surface morphology was investigated by scanning electron microscopy (SEM) ("Tescan FE-SEM"). Other than basic surface morphology electron backscattered diffractometer (EBSD) images and kernel misorientation mappings (KAM) maps were also created to study the physics behind the outcomes. Surface roughness of the unpeened and LPwC processed gears was measured using a confocal microscope of Mahr make "MarSurf CM explorer". An evaluation length of 4 mm and a cut-off length of 0.8 mm were used to evaluate the considered parameters of surface roughness (i.e., the average surface roughness R_a, arithmetic mean height S_a). Analysis of parameters defining the volume of material forming the surface topography analysis such as Vmp, Vmc, Vvc and Vvv was also considered as a part of the investigations.

3. Result and discussion

Table 3 presents values of residual stresses measured by X-ray diffractometer at the root of the gear tooth. The average value of residual stresses for three readings have been used to compare the before LPwC and after LPwC effect on the root of miniature spur gears. It can be seen from Table 3 that maximum improvement in terms of residual stresses (i.e., from 73 MPa tensile to −298.9 MPa compressive) was observed during experiment no. 3 while using 600 mJ as energy and 76.39 J/cm² as fluence. Further, these results were analyzed in detail

with the help of SEM images, EBSD images, and KAM maps in the following sections.

Fig. 4 shows the SEM micrographs of the SLM-manufactured flat sample, mounted gear, and deep exploration of grains in the mounted gear sample. Fig. 4(a) shows the slightly attached granules to the humpy bottom layer. The bottom humpy layer is formed by means of efficiently fused bottom granules. The slight attachment of granules is due to inefficient fusion, which is because of inappropriate melting. Fig. 4(b) shows the SEM micrograph of the mounted gear in resin. However, Fig. 4(c) demonstrates the efficiently merged granules. The efficiently merged granules form a strong bond at the top layer. Whereas it also leads to surface roughness. The surface roughness is studied in the upcoming section. The in-depth investigation of grain orientation is discussed in Fig. 5.

Fig. 5(a, b) shows the KAM orientation and grain orientation plot of the maps recorded by EBSD of the as-built SLM – spur gear. The crystallographic plane from the corresponding pole figure's IPF is shown in figures (c & f), which is found to be [100] in the case of fillet gap and root spots as identified on the top of Fig. 5. The identified spots such as the fillet gap and root in Fig. 5 represent no significant change in planner orientation despite the difference in surface characteristics such as the "stressed" and "stress-free" zone, respectively. The change in surface characteristics is expected due to the difference in transverse laser beam speed while adding layer at identified fillet gap and root spot. The grain area near the fillet gap of the gear profile seems to be long and systematically layered, which is observed in Fig. 5(b). However, the root depicts the refined grains, shown in Fig. 5(e). The refined grain is due to a stress–free zone (surface characteristics) i.e., the end of the root (root). Whereas the fillet gap or root area is in the "concentrated stress zone" lay in the long-layered grains. The kernel-average misorientation (KAM) distribution map is shown in Fig. 5(a and c). The $\langle 100 \rangle$ reveals the misorientation of grain that propagates along with the flakes of grains, which are located near the fillet gap of the gear, and misorientation is found to be <5°. However, near the root misorientation is in the range of 15°. The as-built SEM discussion from the Fig. 4 and grain orientation from the Fig. 5 laid the motif of recorded response to study the influence of LPwC. Fig. 6 demonstrates the influence of LPwC using a hat-top Laser beam in an underwater environment on grain structures using SEM micrographs (fillet gap and root).

The laser-assisted microstructure evolution is dynamic recrystallization in nature, in turn, the type and fluence (J/cm²) of the laser beam interact with the specific geometry of the material. The curved geometry in unpeened samples revealed the presence of high angle grain
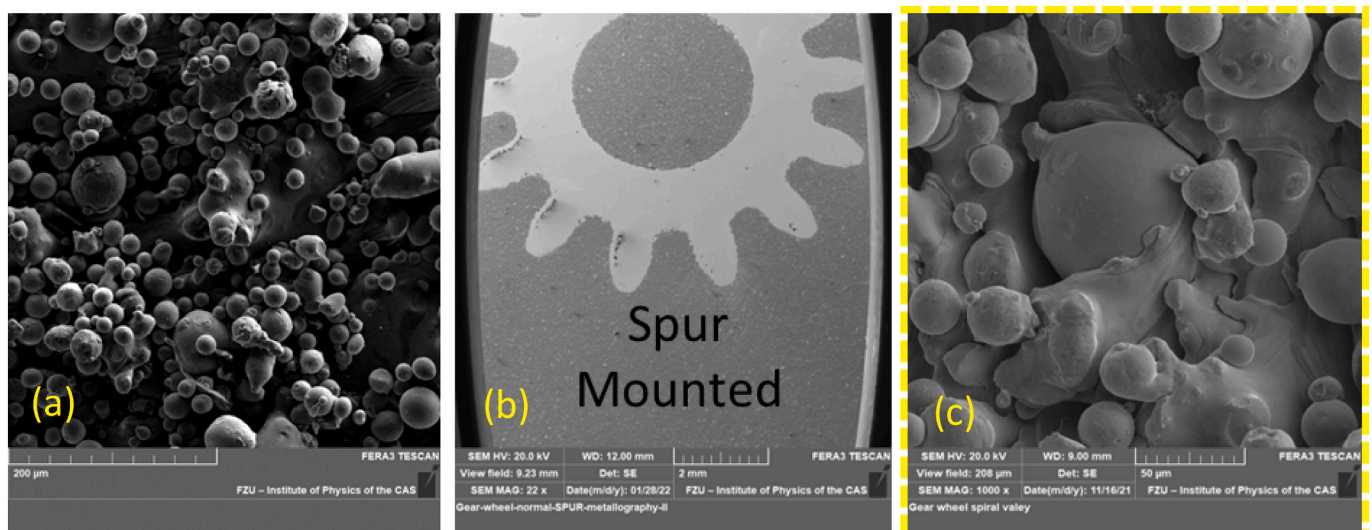

Fig. 4. FE-SEM Micrograph of the (a) flat sample prepared with SLM; (b) spur gear mounted under SEM; and (c) Surface morphology of spur gear fillet area.
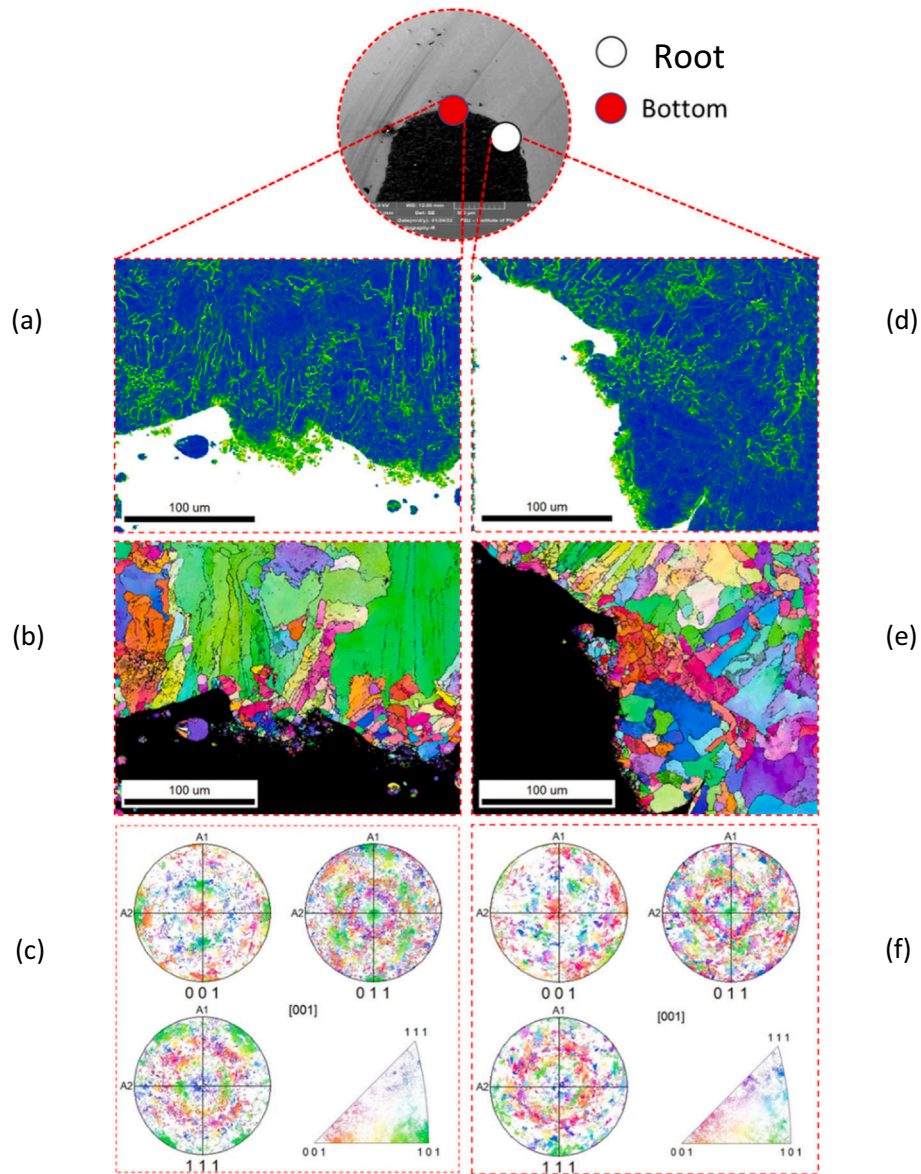
Fig. 5. Spot identification and characterization of unpeened spots using the KAM map, Grain orientation Map, and inverse pole figure at (a–c) fillet gap location, and (d–f) root.
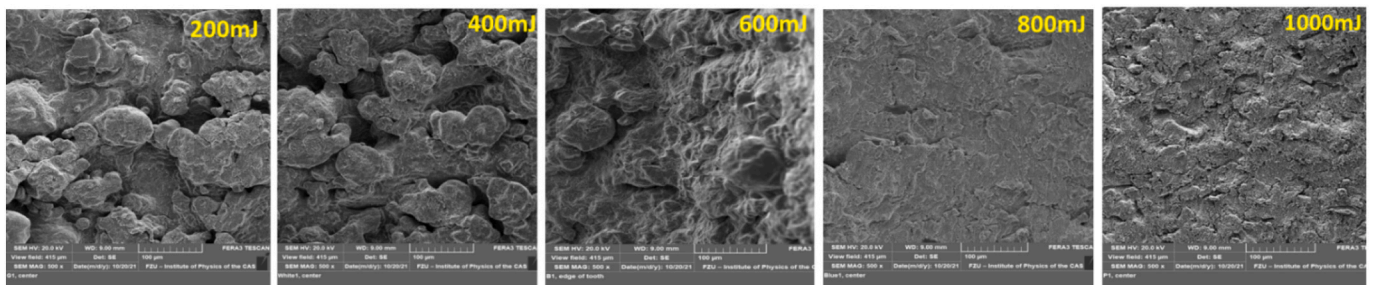

Fig. 6. Shows the FE-SEM of the peened "fillet gap" of the spur gear, the peening was carried out using a circular flat-top beam of wavelength 532 nm and pulse duration of 15 ns, and a repetition rate of 10 Hz. The following laser fluences were used for peening such as (a) 25 J/cm^2, (b) 50 J/cm^2, (c) 75 J/cm^2, (d) 100 J/cm^2, and (e) 125 J/cm^2.

boundaries (HAGBs); shown in Fig. 5. The LPwC using a top-hat circular laser beam in an underwater environment demonstrates an advantage of uniform wave propagation and interaction at the root of SLM-based spur gear. The underwater treatment benefits in confining the plasma for a longer duration and helps in propagating high-pressure shock waves within the fillet and root of the gear at high pulse density and low pulse energy, thus imparting compressive stresses. Fig. 6(a) shows the influence of LPwC using a laser wavelength of 532 nm and fluence of 25 J/
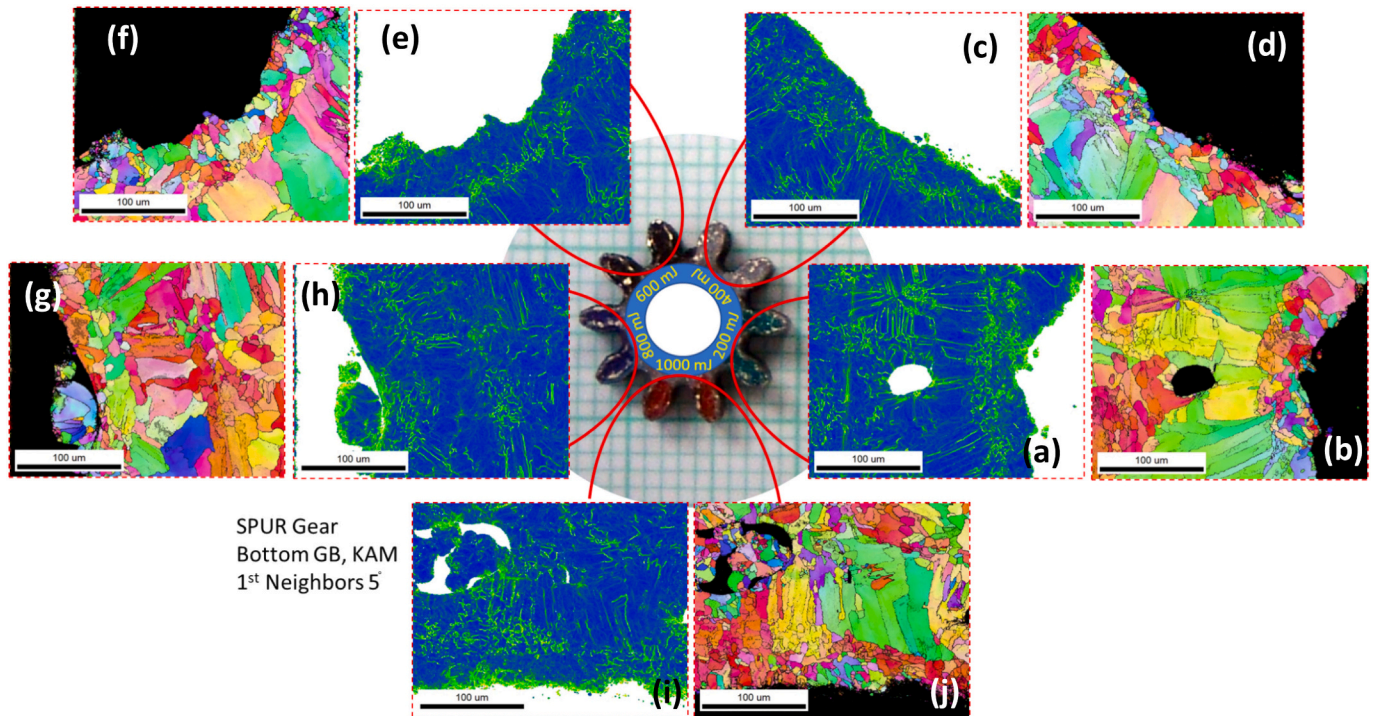
Fig. 7. Demonstrates the influence of laser shock peening using KAM and Grain orientation map at fillet gap at different laser fluences (J/cm^2) such as (a, b) 25 J/cm^2, (c, d) 50 J/cm^2, (e, f) 75 J/cm^2, (g, h) 100 J/cm^2 and (i, j) 125 J/cm^2.
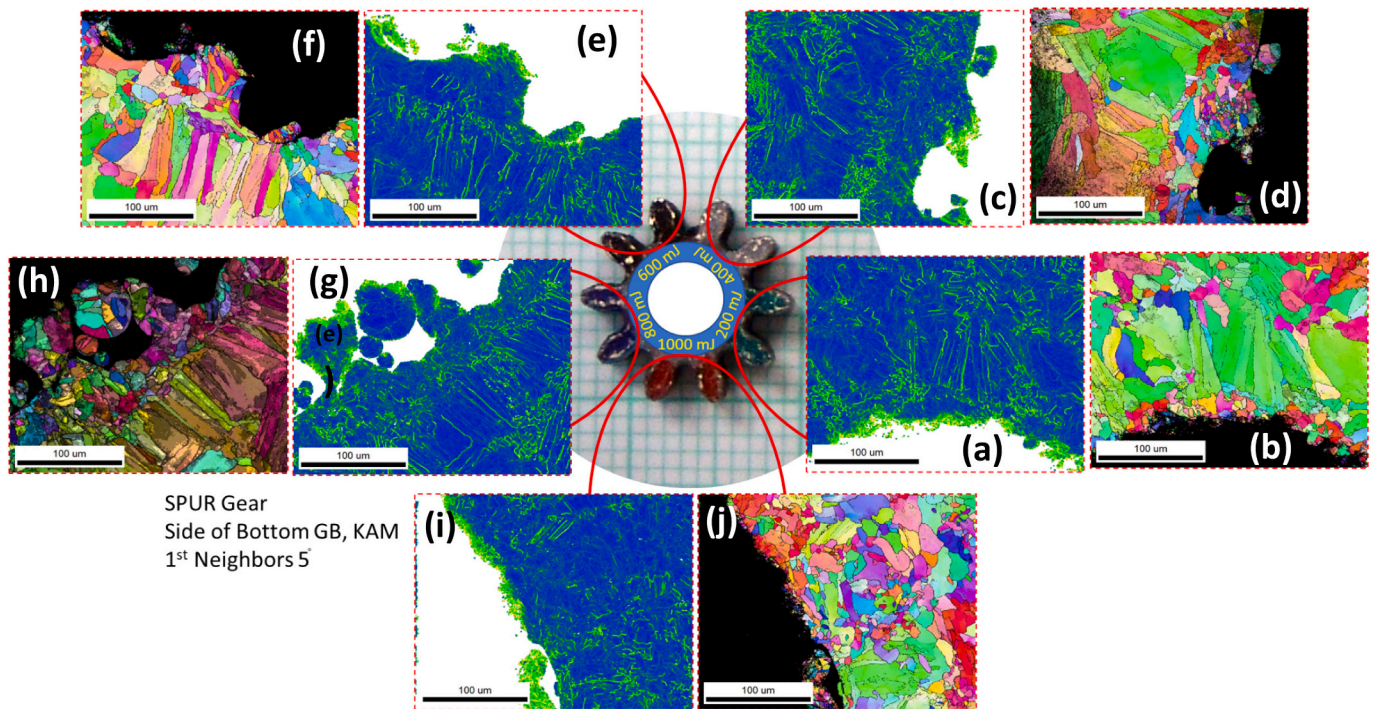

Fig. 8. Demonstrates the influence of laser shock peening using KAM and Grain orientation map of root area at different laser fluences (J/cm^2) such as (a, b) 25 J/cm^2, (c, d) 50 J/cm^2, (e, f) 75 J/cm^2, (g, h) 100 J/cm^2, and (i, j) 125 J/cm^2.

cm^2. The laser fluence unified the fillet gap hump and partially fused the in-efficiently/partially attached granules. While using laser fluence of 50 J/cm^2, the partially attached granules are getting settled in covering the voids, as shown in Fig. 6(b). Fig. 6(c) shows the pronounced influence of laser fluence 75 J/cm^2, which substantiated the bigger partially attached granules into multiple smaller granules and almost completely

fused with a bottom hump layer. The voids are completely covered. Only a few inefficiently attached granules are not fused due to anisotropy in the material characteristics of powder used in SLM. The influence of the top hat circular laser beam is visible i.e., uniformly fused grains over the humpy bottom laser using laser fluence of 75 J/cm^2, shown in Fig. 6(d). However, laser fluence 100 J/cm^2 introduced little perturbation over
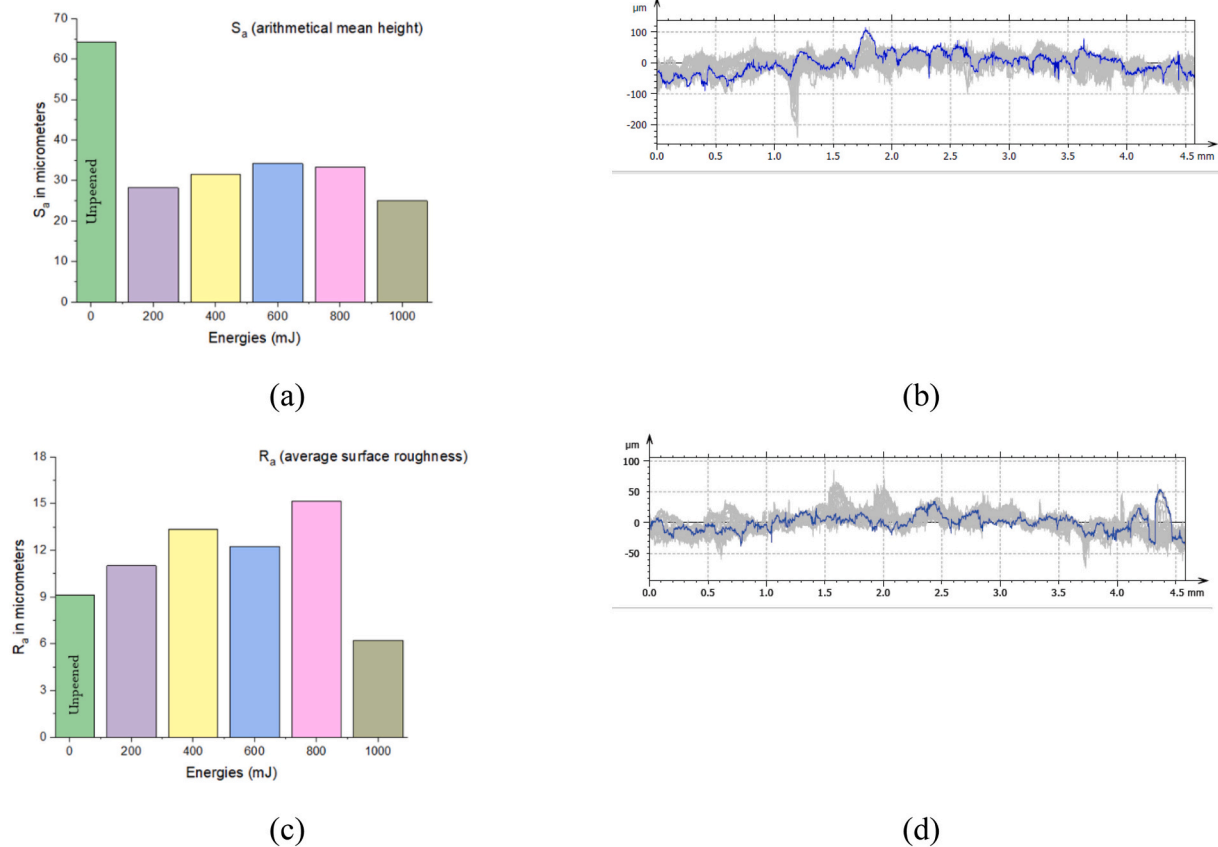
(a)

(b)

(c)

(d)

Fig. 9. Graphical representation of before and after LPwC (a) arithmetical mean height (Sa); (b) average surface roughness (Ra); [(c) and (d)] roughness profile.

the fused surface depicted in Fig. 6(e). Further, the influence of underwater LPwC at grain orientation level is evidenced by employing KAM and IPF by EBSD at fillet gap and root are exhibited in Figs. 7 and 8.

The influence of underwater LPwC in – turn leads to the misorientation of grains is analyzed by the KAM map. In the present work curved geometry at the root of the gear is interacting with the flat top laser beam. The laser interaction transform high angle grain boundaries (HAGBs) into low angle grain boundaries (LAGBs). However, the influence of the curved surface is dominated by the interaction of higher laser fluence. Thus, LPwC below critical fluence [76.39 J/Cm^2] generates concentrated LAGBs and above critical fluence, it generates homogeneously distributed LAGBs. The LAGB's employing hat–top laser beam generates multifold dislocation causing an increase in density. The multifold dislocation occurs within the grain. Within grain, dislocation generates sub-grain. The sub-grain formation substantially inhibits further nucleation and crack propagation owing to an increase in grain boundary density. The sub-grain formation leads to long flake microstructure evolutions in LAGBs. The enhancement in LAGB's percentage increases the mechanical characteristics of the LPwC processed components due to plastic deformation in sub-grains at different orientation angles. The KAM map of the laser fluence 25 J/cm^2 interacted at the fillet gap/root zone of the spur gear shows a higher misorientation density. The higher and dense misorientation is up to the depth of 50 μm shown in Fig. 9(a). The misorientation is confined at the core of the root of the spur gear and reduces towards the outer periphery i.e., the stress-free root. Fig. 9(b) depicts that grain refinement is also observed near the center. Away from the center, the grain size is increasing. Despite the circular top-hat beam, the laser interaction causes an index of refinement due to the arched surface at the gear root. For laser fluence 50 J/cm^2 grain refinement is percolated in uniformity up to a depth of 45–50 μm shown in Fig. 9(d). Fig. 9(c) demonstrates uniformly distributed high angle misorientation density. For laser fluence 75 J/cm^2 the

misorientation is stacked in the top and bottom levels within the band of 50 μm. The laser fluence 75 J/cm^2 reached the threshold to over overcome the influence of curvature in aligning the grain refinement, however it aligned the front and back of the band. Laser fluence 100 J/cm^2 demonstrates a reflection of wave and refocus bur forming a double distinguished band of grain refinement percolation at 25 μm and 100 μm. In a similar way, the laser fluence 125 J/cm^2 shows re-reflection and interaction however reflected wave could push the band to 20 μm, whereas the first reflection pushed the band to the depth of 125 μm. The grain got elongated and layered uniformly without experiencing much misorientation. Post-primary band formation the laser fluences range from 25 to 125 J/cm^2 revealed the influence of the curvature. Influence of curvature and interacted laser fluence divided the extended band into two half that is underside misorientation and upside misorientation. The downside and upside misorientation are observed using laser fluence 25, 75, and 125 J/cm^2. Whereas using 50 J/cm^2 and 100 J/cm^2 shows a mix of upside and downside grain misorientation. Localized deformation plays a vital role in imparting mix upside and downside grain orientation.

The case of the influence of underwater LPwC on grain of the "*root*" spot is studied in detail using the KAM maps. The hat-top laser beam interacts tangentially with the fillet gap's side. By employing flat top laser fluence of 25 J/cm^2 Fig. 8(a) demonstrates the high angle of misorientation on the top side i.e., within a range of 10 μm. However, due to the stress-free zone (top surface), the percolation of the misorientation is uniform. Fig. 8(b) shows the uniform long flakes with low misorientation till the depth of 150 μm. The high misorientation with low grain refinement is observed due to the tangential interaction of the hat-top laser beam with the root. Whereas in the case of laser fluence 50 J/cm^2 demonstrated in Fig. 8(c, d) and tangential interaction leads to inefficient coupling of laser fluence, in turn, generates a high angle of misorientation with random grain refinement till the depth of 50 μm.

Parameters	Value	Unit
Vmp	11.60	µm³/µm²
Vmc	65.98	µm³/µm²
Vvc	138.8	µm³/µm²
Vvv	5.149	µm³/µm²

(a)

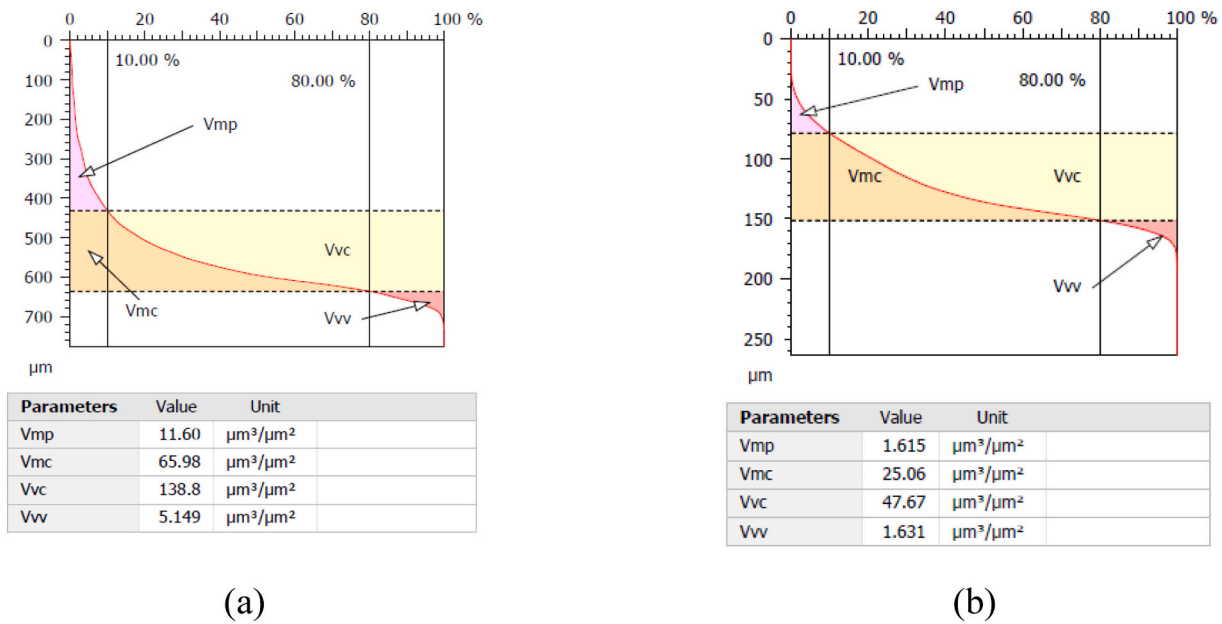| Parameters	Value	Unit
Vmp	1.615	µm³/µm²
Vmc	25.06	µm³/µm²
Vvc	47.67	µm³/µm²
Vvv	1.631	µm³/µm²

(b)

Fig. 10. Material ratio curve for (a) before LPwC and; (b) after LPwC.

The employed laser fluence 75 J/cm^2 shown in Fig. 8(e, f) substantiated the low angle misorientation in long layered flakes without any grain refinement. The low-angle misorientation in long layered flakes contributes to high bond strength and reduced twinning effect [17–20]. A similar influence was observed using hat top laser fluence of 100 J/cm2, as depicted in Fig. 8(g, h). However, long layered flat flakes are dangled with top-side high-angle misorientation and grain refinement. Fig. 8(i, j) shows the uniform grain refinement with the low angle of misorientation perturbed up to 150–200 µm.

3.1. Analysis of surface roughness and material ratio curves

The surface roughness and material ratio curves of the unpeened and LPwC gears were measured. The surface roughness has been measured in terms of two major parameters i.e., Sa (arithmetic mean height) and Ra (average surface roughness), whereas the materials ratio curve was analyzed by analyzing the values of peak material volume (Vmp), core material volume (Vmc), dale void volume (Vvv) and core void volume (Vvc). The results have shown considerable improvement in all the considered parameters except the few cases Ra as shown in Fig. 9(c). In the case of volumetric parameters, it can be seen on comparing Fig. 10 (a) [unpeened] and Fig. 10(b) [LPwC treated] that the values of Vmp. Vmc, Vvc and Vvv have significantly reduced by over 50 % and more. The mentioned improvements were because during the LPwC the high-pressure shock waves pushed the inefficiently attached grains, as seen in Fig. 4(c), to make the surface flatter, as seen in 6(a–e). The voids and craters have been filled, and the surface has become smoother. Such improvements in surface roughness and materials ratio curves are essential to improve the surface quality of the gears, and these improvements will eventually help in better performance of the gears.

4. Conclusions

The present work discussed the outcome on the effects of LPwC on SLM manufactured SS-316L meso sized gears. This work proves that underwater peening of meso sized spur gear without protective taping or coating can be used to alter the surface characteristics of the root along with the fillet radius and space between the teeth. The following conclusions can be drawn:

- LPwC improves the compressive residual stresses from +73 MPa to −298 MPa at 600 mJ/76.49 J/cm^2 of energy/laser fluence.
- It was observed that LPwC is capable of improving the arithmetical mean height "Sa" and peak material volume "Vmp" by over 50 %.
- Improved morphology has been observed in SEM and the unfused particles during SLM were duly placed in the voids and surface has been seen flattened after LPwC compared to Unpeened. The EBSD and KAM maps confirm the grain refinements and shift in misorientation angle. Moreover, the HAGBs transforms to LAGBs.
- LPwC performed without affecting the macro and micro-geometry of the spur gears, as the flank surface of the gear tooth was not altered during LPwC.

Declaration of competing interest

The authors declare the following financial interests/personal relationships which may be considered as potential competing interests: Sunil Pathak reports financial support, administrative support, article publishing charges, and equipment, drugs, or supplies were provided by European Structural and Investment Fund and The Czech Ministry of Education, Youth and Sports. Sunil Pathak has patent pending to LU 502626.

Acknowledgement

References

[1] LU Patent, Office de la propriété intellectuelle: Method for improving surface integrity of an additive manufactured mesoscopic gear, product thereof and device carrying out the method (application number: LU502626).
[2] Wang Y, Pan X, Wang X, et al. Influence of laser shock peening on surface integrity and tensile property of high strength low alloy steel. Chin J Aeronaut 2021;34(6): 199–208.

[3] Attolico MA, Barile C, Casavola C, et al. Effects of laser shock peening on surface roughness and residual stress of AA 7050–T7451. J Mater Eng Perform 2022. https://doi.org/10.1007/s11665-022-06857-7.

[4] Pathak S, Zulić S, Kaufman J, et al. Post-processing of selective laser melting manufactured SS-304L by laser shock peening. J Mater Res Technol 2022;19: 4787–92.

[5] Zulić S, Rostohar D, Kaufman J, et al. Fatigue life enhancement of additive manufactured 316l stainless steel by LSP using a DPSS laser system. Surf Eng 2022; 38(2):183–90.

[6] Zulić S, Fitzmire M, Asadi E, et al. Improvements of metal additive manufactured AISI 304L and Ti6Al4V parts by using laser shock peening as a post-process technique. In: Proc. SPIE 11992, Laser 3D Manufacturing IX. 119920B; 4 March 2022. https://doi.org/10.1117/12.2623654.

[7] Munther M, Martin T, Tajyar A, Hackel L, Beheshti A, Davami K. Laser shock peening and its effects on microstructure and properties of additively manufactured metal alloys: a review. Eng Res Express 2020;2:1021–36.

[8] C. Zhang D. Yalin C. Ye Recent developments and novel applications of laser shock peening: a review, Adv Eng Mater, doi:10.1002/adem.202001216.

[9] Mukai N, Aoki N, Obata M, Ito A, Sano Y, Konagai C. Laser processing forunderwater maintenance in nuclear plants. In: 3rd JSME/ASME Joint International Conference on Nuclear Engineering. 3; 1995. p. 1489–94.

[10] Nataraj MV, Swaroop S. Effect of laser peening without coating on mechanical and microstructural behaviour of SS 304 stainless steel. Mater Today Commun 2022; 33:104200. https://doi.org/10.1016/j.mtcomm.2022.104200.

[11] Luo X, Dang N, Wang X. The effect of laser shock peening, shot peening and their combination on the microstructure and fatigue properties of Ti-6Al-4V titanium alloy. Int J Fatigue 2021;153:106465.

[12] Lan L, Xin R, Jin X, et al. Effects of laser shock peening on microstructure and properties of Ti–6Al–4V titanium alloy fabricated via selective laser melting. Materials 2020;13:3261. https://doi.org/10.3390/ma13153261.

[13] Jose B, Patil T, Rajan SSK, et al. Effect of laser shock peening without coating (LPwC) on a surface and sub-surface characteristics of aged Ti 15 V-3Al- 3Cr-3Sn alloy. Mater Today: Proc 2021;46(Part 1):578–82.

[14] Zhou J, Zhou X, Li H, et al. In-situ laser shock peening for improved surface quality and mechanical properties of laser-directed energy-deposited AlSi10Mg alloy. Addit Manuf 2022;60(Part A):103177. https://doi.org/10.1016/j.addma.2022.103177.

[15] Dudley DW. Gear handbook: the design, manufacture, and application of gears. New York: McGraw-Hill; 1962.

[16] Vrancken B, Thijs L, Kruth J-P, Humbeeck JV. Heat treatment of Ti6Al4V produced by selective laser melting: microstructure and mechanical properties. J Alloys Compd 2012;541:177–85.

[17] Simonelli M, et al. J Phys: Conf Ser 2012;371:012084.

[18] Ding J, Zhang SL, Tong Q, et al. The effects of grain boundary misorientation on the mechanical properties and mechanism of plastic deformation of Ni/Ni3Al: a molecular dynamics study. Materials (Basel) 2020 Dec 15;13(24):5715. https://doi.org/10.3390/ma13245715.

[19] A.l. Mangour BA. Additive manufacturing of high-performance 316L stainless steel nanocomposites via selective laser melting. 2017. PhDT.

[20] Bishara H, Lee S, Brink T, Ghidelli M, Dehm G. Understanding grain boundary electrical resistivity in Cu: the effect of boundary structure. ACS Nano 2021;15(10): 16607–15. https://doi.org/10.1021/acsnano.1c06367.